

A Continuum Theory for Unstructured Mesh Generation in Two Dimensions

Guy Bunin

Department of Physics, Technion,
Haifa 32000, Israel
buning@tx.technion.ac.il

January 30, 2019

Abstract

A continuum description of unstructured meshes in two dimensions is proposed. In the limit of an increasingly finer mesh (smaller cells), and away from irregular vertices, the meshes described have ideally-shaped cells (squares or equilateral triangles). The continuum description has two components. The first is a Riemannian manifold, completely defined by a single real function ϕ on the domain, interpreted as minus the logarithm of the local cell-size. The second component is a family of geodesics on the manifold, along which the edges of the mesh are laid. The conditions for boundary alignment of the geodesics are analyzed. The function ϕ is shown to obey the Poisson equation, with localized charges corresponding to irregular vertices. The problem of finding a suitable manifold for a given domain is thus shown to *exactly* reduce to an Inverse Poisson problem on ϕ , of finding a distribution of localized charges adhering to the conditions derived for boundary alignment. Possible applications to mesh generation are discussed.

1 Overview

A mesh is a partition of a domain into smaller parts, typically with simpler geometry, called cells. In two dimensions, cells are usually triangles or quadrilaterals. The shapes of the cells may be important; for many applications, cells with shapes similar to an equilateral triangle or square are preferred. The problem of mesh generation can then be seen as an optimization problem: to find a partition of a domain into well-shaped cells, possibly under additional demands, such as cell size requirements.

The mesh generation problem has been the subject of extensive research. Many techniques for creating meshes exist, especially in two dimensions [1],[2]. Nevertheless, some of the most popular techniques, which create good meshes in many cases, are heuristic in nature, and may create less than optimal meshes

for some inputs. Two of the inherent characteristics of the mesh generation problem seem to make it very difficult to solve:

- (i) The constraints on cells' shapes are *global*. That is, the shape of a cell somewhere in the domain is constrained by the possible shapes of its neighbors, which in turn are constrained by the shapes of their neighbors, and so on. Thus, at least in principle, the constraints on the mesh layout extend over the whole domain (or more precisely, over each connected component of the domain).
- (ii) The problem combines *discrete and continuous aspects*. The number of cells and the mesh connectivity (i.e.: which cells are neighbors? which faces do they share?) are of discrete nature, whereas the locations of the vertices can vary continuously. These aspects are closely intertwined, preventing the sole use of purely discrete techniques (algebraic, graph-theoretic, etc.), or techniques designed for use in problems of continuous nature.

Mesh generation algorithms can be divided into those creating structured meshes, and those creating unstructured meshes. A structured mesh is a mesh whose connectivity is that of a regular grid, see Fig. 1,(iii). Since the connectivity of the mesh (the discrete aspect of the problem) is assumed beforehand, Characteristic (ii) above is considerably simplified. One way of assigning locations to the mesh vertices is by finding a function that maps the domain of the regular grid to the domain to be meshed, and using it to map the vertices. For a survey, see Ref. 2. Advanced differential geometry methods have also been used in mapping techniques [3]. For small enough cells, the differential properties of the mapping function at the cell's location then dictate its shape. If, for example, a mapping is conformal, i.e. angle preserving, then the inner angle of a small enough cell will be approximately preserved under the mapping.

A different approach to mesh generation is offered by unstructured mesh generation methods [1]. As an example of this category, advancing-front algorithms have enjoyed great popularity. Advancing-front algorithms start from the boundaries and lay one cell, or one layer of cells, at a time. This can be viewed as an approximation of the global constraints (Characteristic (i) above) by a series of local problems. In contrast to structured mesh generation, where the connectivity of the mesh is that of an "ideal" grid, possibly at the expense of the cells' shapes throughout the mesh, in advancing-front techniques an attempt is made to lay well-shaped cells as much as possible, at the price of creating irregular nodes, where mesh connectivity is not that of a perfect grid, see Fig. 1,(ii). This, of course, affects the cells' shapes.

The present work is concerned with a continuum description of unstructured meshes of two-dimensional, planar domains. This description can be thought of, roughly, as the analog of the mapping function in mapping techniques, in a sense that it is better approximated by meshes with smaller cells. In the spirit of unstructured meshing, the theory aims at describing meshes having well-shaped cells, at the expense of introducing irregular vertices into the mesh. In fact, we demand that in the limit of an increasingly finer mesh, the cells, at a given

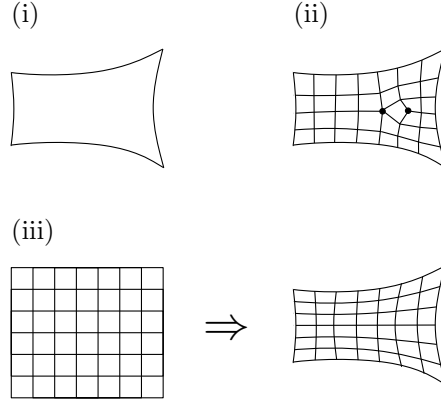


Figure 1: Unstructured vs. structured meshes. (i) Input domain. (ii) Unstructured mesh. Irregular vertices are marked. (iii) Structured mesh created by mapping a regular grid.

point which is not an irregular vertex, *approach the shape of an “ideal” cell* (i.e. equilateral triangle or square). This demand, which will be referred to as the “ideality” demand, allows one to define a local cell size at every point (since the cells have unit aspect ratio). Local edge direction can also be defined. In the quadrilateral mesh case, this direction is defined up to additions of $\pi/2$ radians (since due to the “ideality” demand the edges form right angles at incidence), or $\pi/3$ radians in the triangular case. When local cell size and local cell direction are translated to mathematical quantities, the “ideality” demand can be used to derive differential relations governing the changes of these quantities.

The mathematical formulation of the above concepts is done within the framework of differential geometry. More specifically, the domain to be meshed is bestowed with a Riemannian manifold structure. A Riemannian manifold is a generalization of the concept of a surface, in which the metric can be taken as a fundamental entity, and used to calculate the distance between points on the manifold. The link with the final mesh structure will be made by demanding that a *cell-edge have unit length* on the manifold (exact only in the limit of a fine mesh, i.e. small cells).

The manifold discussed will be assumed to have the following two main properties:

- (i) The manifold is locally flat everywhere, except at singularities. (A “flat” region can be imagined as a bent, but not stretched, piece of paper.) Singularities will correspond to irregular vertices, see below.
- (ii) A real function ϕ is defined in the domain (except at singularities), such that at any given point the matrix $(g_{ij})_{1 \leq i,j \leq 2}$, composed of the metric coefficients, is proportional to the identity matrix: $g_{ij} = e^{2\phi} \delta_{ij}$, where δ_{ij}

is the Kronecker delta. We stress that the proportionality $e^{2\phi}$ can vary throughout the domain. The quantity $e^{-\phi}$ will be interpreted as the local cell size. (In manifold theory terminology, if $g_{ij} \propto \delta_{ij}$, the coordinates are known as a “conformal parametrization” of the manifold.)

These two properties are motivated by the following: Property (i) ensures that locally, at some region of the domain that does not include a singularity, a “grid” of orthogonal geodesics can be constructed. Due to Property (ii) the cells formed by the crossing geodesics of the grid will be of regular shape (unit aspect ratio) in the continuum limit.

The mathematical formulation of property (i) is that the curvature tensor of the manifold be identically zero everywhere, except at conical singularities. Combined with the equation $g_{ij} = e^{2\phi} \delta_{ij}$ of property (ii), the two formulas give a remarkably simple result, viz. that ϕ must obey the Laplace equation $\nabla^2 \phi = 0$. This is a well known result in general relativity, see section 2.

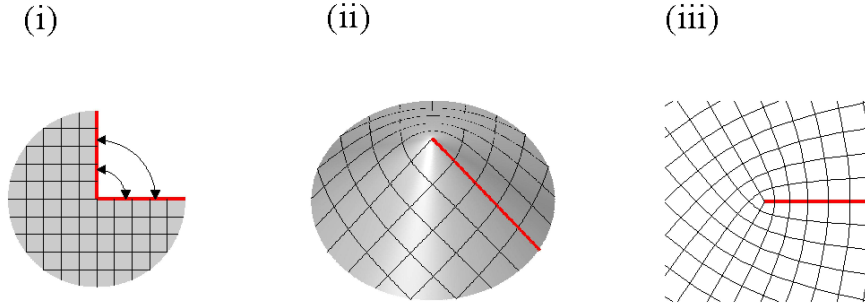


Figure 2: Conical singularity. (i) The Volterra construction. (ii) A cone created by the Volterra construction. (iii) Geodesics on a manifold containing a conical singularity.

An irregular node is then described by a conical singularity, as can be visualized using the Volterra construction¹. Imagine a piece of paper with an angular section cut out, see Fig. 2,(i). If the two edges of the section are identified, i.e. glued together, the paper will assume the shape of a cone, see Fig. 2,(ii). A manifold is a generalization of the concept of a surface, and a manifold on the plane “representing” the same surface as the cone (i.e. isometric to a cone) can be constructed, see Fig. 2,(iii)². In this illustration the curves are the images of geodesics (the manifold-analog of straight lines) of the manifold. The

¹See Ref. 4, as cited by Ref. 5.

²Strictly speaking, the “tip” of the cone is not part of the Riemannian manifold.

spacing between the geodesics is one manifold distance. The term *defect* will be used interchangeably with the term conical singularity, having exactly the same meaning (this is the standard terminology in the “theory of defects” of physics and material sciences, see e.g. Ref. 11).

A large portion of the work is then devoted to defining local mesh direction, and analyzing the requirement that the mesh conform to the boundary, i.e. that the boundary be composed of cell edges, see Fig. 3. To this end, a family of geodesics called the *C-frame* is defined. The C-frame geodesics cross each other at the desired angle between edges ($\pi/3$ for triangles and $\pi/2$ for quadrilaterals), and conform to the boundary, see Fig. 3. The existence of a C-frame is translated to conditions on ϕ . Additional requirements, such as edge-size on boundary, can also be formulated.

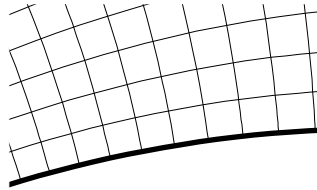


Figure 3: Boundary alignment. Boundary marked with heavy line.

The main result of the present work is that for a C-frame to exist the function ϕ , which completely defines the manifold, has to obey the Poisson equation $\nabla^2\phi = \rho$, with ρ being a sum of “localized charges” (Dirac delta functions). The charges are placed at the conical singularity locations, thus corresponding to the irregular vertices of the mesh. The charge strength is related to the cone excess angle (the difference between the cone angle and 2π) corresponding to the number of cells incident on the irregular vertex. For example, in the manifold shown in Fig. 2,(iii), the conical singularity has a excess angle of $-\pi/2$. The charge of the singularity, located at $r = 0$, corresponding to such a excess angle is $-\frac{\pi}{2}\delta^{(2)}(r)$, where $\delta^{(2)}(\cdot)$ is the Dirac delta function in two dimensions. This is the charge of any singularity corresponding to an irregular vertex surrounded by three cells. Along with the boundary alignment conditions on ϕ , the problem of finding an appropriate manifold is thus reduced to an *Inverse Poisson* problem, of finding a charge distribution adhering to these conditions. The reduction gives *exact, global* relations that the manifold must obey.

Conformal parametrization of manifolds with conical singularities have been used in surface parametrization problems [6]-[9]. The two dimensional mesh generation problem with boundaries is different from the surface parametrization

problem, because of the boundary alignment requirement in mesh generation. In fact, the parametrization problem for planar domains is trivial: the coordinates of the plane form a good parametrization. This parametrization, however, does not solve the mesh generation problem. Ref. [8] describes an algorithm that accepts input local directions in the form of a pair of orthogonal vector fields. A parametrization with singularities, as tangential as possible to the vector fields, is sought. The required cell size is either constant (termed “normal spacing”), or, as is described in section 4.1 of Ref. 8, preprocessed so that using the local direction given by the input vector fields, fewer singularities are created (the “curl correction” process). In contrast, our work investigates the case where both local mesh direction and local cell size inside the domain are initially unknown, and treated at once, as conditions for placing conical singularities are derived, so that boundary alignment requirements, and optionally boundary cell size requirements, are met.

In what follows, the structure and machinery of differential geometry are used. Geodesics and parallel transport concepts are extensively used. The necessary material can be found in any textbook on the subject, such as Ref. 10.

The rest of the article is organized as follows: In section 2 the ϕ -manifold is defined. In section 3 the differential equations obeyed by geodesics and parallel transport on the manifold are derived. Section 4 introduces the concept of a C-frame. The necessary and sufficient conditions for the existence of a C-frame are developed in sections 5 and 6. This set of conditions forms the core result of the work. In section 7 the theory is discussed through three case studies. Case Studies A,B are used to discuss the meaning of the conditions derived before. In Case Study C the possible structure of a mesh generation algorithm is discussed. An example quadrilateral mesh problem, though admittedly simple and artificial, demonstrates how, given an input, a manifold with defects is constructed, adhering to the imposed conditions. This manifold allows the construction of meshes with irregular vertices; at any given point in the domain that is not an irregular vertex, at the limit of increasingly finer meshes, the cells’ shapes tend to a square.

2 Definition of the Manifold

The input to the mesh generation problem is assumed to be a bounded open domain $D \subset \mathbb{R}^2$ such that:

- (i) Its boundary ∂D is a union of a finite number of connected components

$$\partial D = \cup \Gamma_j.$$
- (ii) Every component Γ_j is a piecewise C^2 closed curve.

The points where a boundary component Γ_j is not differentiable will be called *junction points*. The set of all junction points will be denoted by J .

Let P be a finite set of points in D , and P_B a finite set of points in $\partial D \setminus J$. (The points in P will be the locations of the conical singularities, see below and in section 1. The points P_B will be the locations of boundary singularities.) We now turn to study the following class of Riemannian metrics.

Definition 1 (ϕ -manifold) *A ϕ -manifold is a Riemannian manifold defined on $D \setminus P$, such that:*

- (i) *It is locally flat, i.e. the curvature tensor $R_{i\ kl}^j = 0$ for all points in $D \setminus P$.*
- (ii) *The metric $g_{ij} = e^{2\phi} \delta_{ij}$ where ϕ is a real function on $D \setminus P$ that is sufficiently smooth, and δ_{ij} is the Kronecker delta.*
- (iii) *For every boundary point $A \in \Gamma_j$, $A \notin J \cup P_B$, the limits $\lim_{r \rightarrow A} \phi(r)$ and $\lim_{r \rightarrow A} \nabla \phi(r)$ exist and are continuous along Γ_j at A .*

Combining items (i),(ii) of the ϕ -manifold definition, a differential equation for ϕ can be found. In two dimensions, there is just one independent non-trivial component of the curvature tensor $R_{i\ kl}^j$, which can be taken to be $R_{1\ 12}^2$. Substituting $g_{ij} = e^{2\phi} \delta_{ij}$ into the equation $R_{1\ 12}^2 = 0$ yields

$$0 = \frac{\partial^2 \phi}{\partial x^2} + \frac{\partial^2 \phi}{\partial y^2} = \nabla^2 \phi \quad (1)$$

where $(x, y) = (x^1, x^2)$. The definition of $R_{i\ kl}^j$ is reproduced in Appendix A, in which an alternative derivation of Eq. (1) is also given.

Since $R_{1\ 12}^2$ is the only independent component of the curvature tensor, Eq. (1) is also a sufficient condition for local flatness. Given the complexity of the curvature tensor definition, Eq. (1) is remarkably simple. It is a well known result in general relativity^{3,4}.

Remark 2 *The angle between two vectors on a manifold $x = (x^1, x^2), y = (y^1, y^2)$ is given by $\cos \theta = (x^i g_{ij} y^j) / (\sqrt{x^i g_{ij} x^j} \sqrt{y^k g_{kl} y^l})$. The Einstein summation convention is applied here and throughout the text. On a ϕ -manifold, where $g_{ij} = e^{2\phi} \delta_{ij}$, this is equal to $\cos \theta = (x^i y^i) / (\sqrt{x^i x^i} \sqrt{y^j y^j})$, which is the “coordinate”, or “Euclidian” definition of an angle. In what follows these two equivalent definitions will be referred to as the “angle” between vectors. This definition will also be used for measuring angles between vectors relating to different points on the manifold (which is well defined only for the Euclidian manifold). The distance on the ϕ -manifold will be denoted by l , $dl^2 = dx^i g_{ij} dx^j$. Euclidian distance will be denoted by s , $ds^2 = dx^i dx^i$.*

³See Ref. 11, and references therein. In Ref. 11 this equation is presented in the context of the theory of elasticity, which is closer to the present work than that of general relativity.

⁴Although the Laplace equation is shared by both, Eq. (1) should not be confused with the “Laplacian smoothing” procedure [12]. In Laplacian smoothing, ϕ are the coordinates of vertices in the “physical” domain, taken functions of their location in the “logical” domain. In Eq. (1), ϕ is minus the logarithm of the local-cell-size, written as a function of the “physical” domain location, and no “logical” coordinates are defined.

3 Geodesics, Parallel Transport

In this section the equations for geodesics and parallel transport on a ϕ -manifold are derived. The geodesic curve is the analog of a straight line for manifolds. If $\gamma(t) = (\gamma^1(t), \gamma^2(t))$ is a geodesic curve, it satisfies the following equations for $k = 1, 2$

$$0 = \frac{d^2\gamma^k}{dt^2} + \Gamma_{ij}^k \frac{d\gamma^i}{dt} \frac{d\gamma^j}{dt} \quad (2)$$

where Γ_{ij}^k is Christoffel's symbol, and the summation convention is applied. Γ_{ij}^k is given by

$$\Gamma_{ij}^l = \frac{1}{2} g^{kl} \left(\frac{\partial g_{ik}}{\partial x^j} - \frac{\partial g_{ij}}{\partial x^k} + \frac{\partial g_{kj}}{\partial x^i} \right). \quad (3)$$

where g^{kl} is the (k, l) entry of the inverse of the matrix (g_{ij}) . Noting that in a ϕ -manifold $g^{kl} = e^{-2\phi} \delta^{kl}$ we get, after some algebra, the following equations for the components of $\gamma(t)$:

$$\begin{aligned} 0 &= \frac{d^2\gamma^1}{dt^2} + 2 \left(\frac{\partial\phi}{\partial x^1} \frac{d\gamma^1}{dt} + \frac{\partial\phi}{\partial x^2} \frac{d\gamma^2}{dt} \right) \frac{d\gamma^1}{dt} - \frac{\partial\phi}{\partial x^1} \left(\left(\frac{d\gamma^1}{dt} \right)^2 + \left(\frac{d\gamma^2}{dt} \right)^2 \right), \quad (4) \\ 0 &= \frac{d^2\gamma^2}{dt^2} + 2 \left(\frac{\partial\phi}{\partial x^1} \frac{d\gamma^1}{dt} + \frac{\partial\phi}{\partial x^2} \frac{d\gamma^2}{dt} \right) \frac{d\gamma^2}{dt} - \frac{\partial\phi}{\partial x^2} \left(\left(\frac{d\gamma^1}{dt} \right)^2 + \left(\frac{d\gamma^2}{dt} \right)^2 \right). \end{aligned}$$

These two equations can be written in vector notation as

$$0 = \frac{d^2\gamma}{dt^2} + 2 \left(\frac{d\gamma}{dt} \cdot \nabla\phi \right) \frac{d\gamma}{dt} - v^2 \nabla\phi \quad (5)$$

with $v \equiv \left| \frac{d\gamma}{dt} \right|$. Let \mathbf{t} be the (unit length) tangent to $\gamma(t)$, and \mathbf{n} be the normal, such that (\mathbf{t}, \mathbf{n}) form a right-handed system, see Fig. 4. Taking the dot-product of Eq. (5) with \mathbf{n} gives

$$\frac{\partial\phi}{\partial n} \equiv \nabla\phi \cdot \mathbf{n} = \frac{1}{v^2} \frac{d^2\gamma}{dt^2} \cdot \mathbf{n} = \kappa \quad (6)$$

where κ is the curvature⁵ of the curve γ . Note that κ can be negative. Thus, the curvature of the geodesic is equal to the normal component of the gradient of ϕ . Eq. (6) can also be put in integral form. Define $\theta_{\mathbf{t}}$ to be the angle between \mathbf{t} and the x-axis (see Notation 2.2). If $\gamma(s)$ is the arc length parametrization of γ (with the “Euclidian” metric $ds^2 = dx^i dx^i$, see Notation 2.2) then $\kappa = d\theta_{\mathbf{t}}/ds$, and

$$\delta\theta_{\mathbf{t}} \equiv \int_{s_1}^{s_2} \frac{d\theta_t}{ds} ds = \int_{s_1}^{s_2} \kappa ds = \int_{s_1}^{s_2} \frac{\partial\phi}{\partial n} ds \quad (7)$$

where the integration is carried out along γ from s_1 to s_2 . The expression $\Phi_{\gamma} \equiv \int_{s_1}^{s_2} \frac{\partial\phi}{\partial n} ds$ is recognized as the flux of the field $\nabla\phi$ through γ . Thus, the change in the direction of \mathbf{t} is equal to the flux of $\nabla\phi$ through γ .

⁵ κ is the curvature of γ in \mathbb{R}^2 with respect to the Euclidian metric. The curvature of γ in the ϕ -manifold is zero by definition.

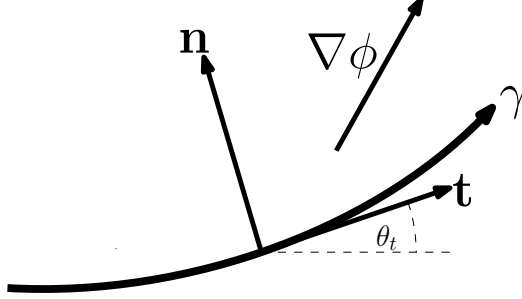


Figure 4: A geodesic curve

The parallel transport of a vector allows the definition of parallel vectors along a given curve. The derivation of the parallel transport equation is similar to that of the geodesic equation. The equation for parallel transport of the components of a vector $\mathbf{y} = (y^1, y^2)$ along a curve $\alpha(t) = (\alpha^1(t), \alpha^2(t))$ is

$$0 = \frac{dy^l}{dt} + \Gamma_{ij}^l y^i \frac{d\alpha^j}{dt}. \quad (8)$$

Note that α does not have to be a geodesic. After substituting the metric into Eq. (8) using the definition of Γ_{ij}^l in Eq. (3) and reordering, the equations can be put in the form

$$0 = \frac{d\mathbf{y}}{dt} - \mathbf{y}_\perp (\nabla\phi \cdot \mathbf{n}) v + \mathbf{y} \left(\nabla\phi \cdot \frac{d\alpha}{dt} \right) \quad (9)$$

where $\mathbf{y}_\perp = (-y^2, y^1)$. To find the change in the direction of \mathbf{y} we take the dot-product of Eq. (9) with \mathbf{y}_\perp and get

$$0 = \frac{d\mathbf{y}}{dt} \cdot \mathbf{y}_\perp - |\mathbf{y}_\perp|^2 (\nabla\phi \cdot \mathbf{n}) v = \frac{d\mathbf{y}}{dt} \cdot \mathbf{y}_\perp - |\mathbf{y}|^2 (\nabla\phi \cdot \mathbf{n}) v. \quad (10)$$

The change in the angle θ_y between \mathbf{y} and the x-axis is given by

$$\frac{d\theta_y}{ds} = \frac{1}{|\mathbf{y}| v} \frac{d\mathbf{y}}{dt} \cdot \frac{\mathbf{y}_\perp}{|\mathbf{y}|} = \nabla\phi \cdot \mathbf{n} = \frac{\partial\phi}{\partial n}. \quad (11)$$

In the second equality, Eq. (10) was used. If α is written in its arc-length parametrization, then integrating Eq. (11) along α from s_1 to s_2 yields

$$\delta\theta_y \equiv \int_{s_1}^{s_2} \frac{d\theta_y}{ds} ds = \int_{s_1}^{s_2} \frac{\partial\phi}{\partial n} ds = \Phi_\gamma \quad (12)$$

where Φ_γ is the $\nabla\phi$ flux through α . Eq. (12) is actually a generalization of Eq. (7), since it is true in general that the tangent vector to a geodesic curve γ is parallel to itself along γ .

4 Crossing geodesics

From this point on, quadrilateral- and triangular-meshes will require slightly different treatments. This stems from the fact that the inner angle of an “ideal” quadrilateral, i.e. a square, is $\pi/2$, whereas for triangles this angle is $\pi/3$. For clarity of presentation, the quadrilateral case is treated first. The slight changes in the results for the triangular case are given in B.

4.1 Definitions

In this section a specific family of geodesics is discussed. Loosely speaking, edges of the mesh will be laid along geodesics of this family. In the intent of creating a mesh with edges of a quadrilateral at approximately right angles, we seek a family F of geodesics defined as follows:

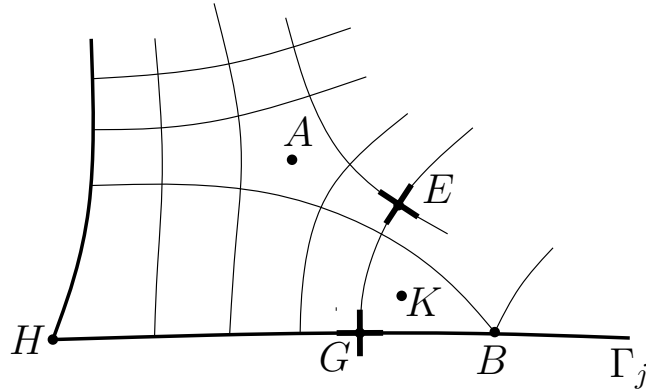


Figure 5: Illustration of a C-frame. Γ_j is a boundary curve. Selected C-frame geodesics are shown (thin lines). $K, A \in P$, $B \in P_B$, $H \in J$. Crosses at E, G are shown.

Definition 3 (C-frame definition) *A family F of geodesics is a continuous-frame (C-frame) if:*

- (i) *Through every point $A \in D \setminus P$ there passes at least one geodesic $\gamma_1 \in F$, and if γ_2 is a geodesic passing through A , then γ_1, γ_2 are parallel or perpendicular at A if and only if $\gamma_2 \in F$.*
- (ii) *If A is a point on a boundary curve Γ_j , $A \notin J \cup P_B$, and $\gamma_1 \in F$ such that $\lim_{t \rightarrow t_0} (\gamma_1(t)) = A$, then γ_1 and Γ_j are parallel or perpendicular at A .*

See Fig. 5 for an illustration of a C-frame. Note that parallel geodesics are equivalent up to change in parametrization and extension of the curves, thus in item (i) of the C-frame definition only two essentially different geodesics pass through each point, see also Fig. 5.

In section 5 the conditions for the existence of a C-frame will be investigated. It is however more convenient to work with parallel transport of tangents to the geodesics along *arbitrary* curves, rather than with the geodesics themselves. In the rest of this section a structure equivalent to a C-frame, the *cross-field*, will be defined and its connection to a C-frame will be established, see Fig. 6.

$$\begin{array}{c}
 \text{C-frame existence} \\
 \Updownarrow \\
 \text{cross-field existence} \\
 \Updownarrow \\
 \text{conditions on } \phi
 \end{array}$$

Figure 6: C-frame existence line of argument.

The geodesics in F define a direction at every point $A \in D \setminus P$, defined up to an addition of $k\pi/2$, $k \in \mathbb{Z}$. This can be visualized as assigning a cross to every point, see Fig. 5. This leads to the definition of a *cross*.

Definition 4 (Cross) *First, define an equivalence \sim of vectors in \mathbb{R}^2 : for 2 vectors $v_1, v_2 \in \mathbb{R}^2$, $v_1 \sim v_2$ if and only if v_1, v_2 are parallel or perpendicular. A cross is an element of \mathbb{R}^2 / \sim .*

Since the angle between vectors is preserved in parallel transport along a given curve [10], the cross equivalence class structure is preserved, and the parallel transport of crosses is well-defined. Moreover, \mathbb{R}^2 / \sim has a topology induced from \mathbb{R}^2 , in which the limit of crosses is well-defined.

Definition 5 *For a curve α , and a point B in the image of α , $\mathbf{t}_B(\gamma)$ is the tangent to γ at B .*

Definition 6 (cross-field) *A cross-field on $D \setminus P$ is a mapping $V : D \setminus P \rightarrow \mathbb{R}^2 / \sim$ such that:*

- (i) *For $A, B \in D \setminus P$, the parallel transport of $V(A)$ to B along a curve α is independent of α and is equal to $V(B)$.*
- (ii) *If $A \in \Gamma_j \setminus (J \cup P_B)$, and α is a curve such that $\lim_{t \rightarrow t_0} (\alpha(t)) = A$, then the tangent $\mathbf{t}_A(\Gamma_j) \in \lim_{t \rightarrow t_0} (V(\alpha(t)))$. Denote: $V(A) \equiv \lim_{t \rightarrow t_0} (V(\alpha(t)))$.*

If $A \in \Gamma_j \setminus (J \cup P_B)$, then the ϕ -manifold definition, (iii), and Picard's theorem [13], [10] ensure that the parallel-transport equation can also be solved uniquely *starting* from A , even though $A \notin D$. This is therefore true for crosses as well.

In what follows, a relation between a C-frame and a cross-field will be established. To this end, the following structure is defined.

Definition 7 (Cross-geodesics) Given a point $A \in D \setminus P$ and a cross $V(A)$ at A , let G be the set of geodesics that pass through A and their tangents are in $V(A)$. Elements of G will be called the cross-geodesics at A . By definition of a cross, every two geodesics in G are either parallel or perpendicular at A .

Claim 8 (Creating a C-frame given a cross-field) If V is a cross-field, and $G(A)$ is the cross geodesics set at A , define a family of geodesics $F \equiv \cup_{A \in D \setminus P} G(A)$. Then F is a C-frame.

Proof. First, we show that item (i) of the C-frame definition holds. Given a point $A \in D \setminus P$, $G(A)$ is not empty, and therefore there is a geodesic γ_1 in F passing through A . To show that every geodesic in F is either parallel or perpendicular to γ_1 , let $\gamma_2 \in F$ which passes through A . Then $\gamma_2 \in G(B)$ for some point B , see Fig. 7. We need to show that $t_A(\gamma_2)$ is parallel or perpendicular to γ_1 , i.e. $\gamma_2 \in G(A)$. $t_B(\gamma_2) \in V(B)$, and is parallel translated to $t_A(\gamma_2)$ along γ_2 . Therefore, by cross-field definition, (i), $t_A(\gamma_2) \in V(A)$, thus $\gamma_2 \in G(A)$.

We turn to show that item (ii) of the C-frame definition holds. If $C \in \Gamma_j \setminus (J \cup P_B)$, and $\lim_{t \rightarrow t_0} (\gamma_1(t)) = C$ then by cross-field definition, (ii), $t_C(\Gamma_j) \in V(C)$. For every point B in the image of γ_1 , $t_B(\gamma_1) \in V(B)$, thus $\lim_{t \rightarrow t_0} t_{\gamma_1(t)}(\gamma_1) \in \lim_{t \rightarrow t_0} (V(\gamma_1(t))) = V(C)$. Since both $t_C(\Gamma_j)$ and $\lim_{t \rightarrow t_0} t_{\gamma_1(t)}(\gamma_1)$ belong to $V(C)$ they are either parallel or perpendicular. ■

The inverse of Claim 4.1 is also true, that is, given a C-frame a cross-field can be constructed. The cross at every point is given by the tangents to the C-frame geodesics at that point; the proof is similar to that of Claim 4.1 and is omitted.

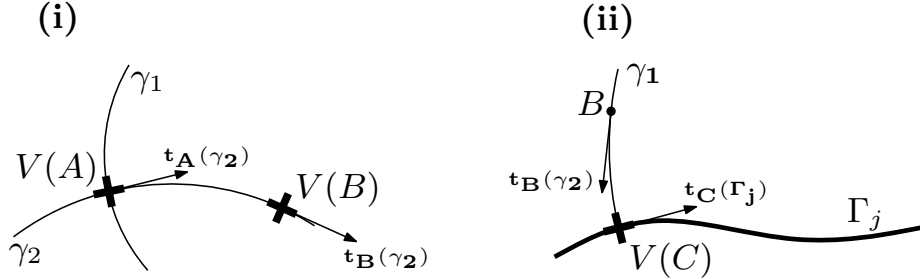


Figure 7: Proof of Claim 4.1.

5 Conditions for the existence of a C-frame

Using claim 4.1, the existence of a C-frame is reduced to the existence of a cross-field. Conditions for the existence of a cross-field V on $D \setminus P$ will now be investigated. We start with the behavior of ϕ near a point $p \in P$. Let $A \in D \setminus P$,

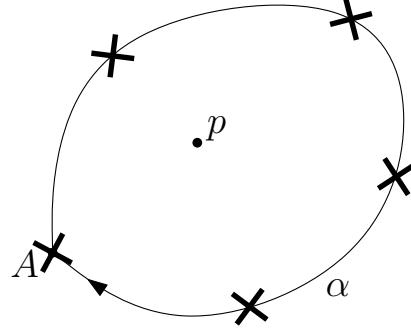


Figure 8: Condition 1A.

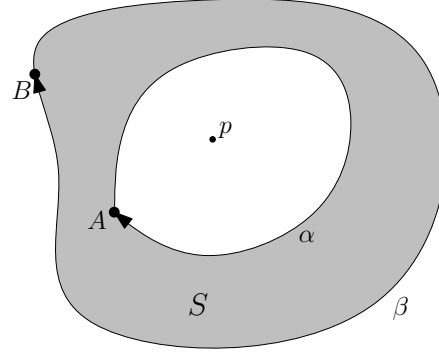


Figure 9: Invariance of the flux through loops enclosing p .

and let α be a simple closed curve starting from A that encloses p , and only p of P , see Fig. 8. According to cross-field definition, $V(A)$ is translated to $V(A)$ along α . A vector $\mathbf{y} \in V(A)$ is parallel translated along α to $\mathbf{y}' \in V(A)$. Thus, \mathbf{y}, \mathbf{y}' are either parallel or perpendicular, and the total variation of \mathbf{y} along α is $\delta\theta_y = k\pi/2$, $k \in \mathbb{Z}$. Using Eq. (12) we get the following condition for the existence of a cross field:

Condition 1A. *The flux of $\nabla\phi$ through a closed curve enclosing a singularity is*

$$\Phi = \delta\theta_y = k\pi/2. \quad (13)$$

Eq. (13) is independent of α , as long as it encloses p only, since $\nabla^2\phi = 0$ elsewhere: if β is another path enclosing p only, and S is the area between α and β , see Fig. 9, then

$$0 = \int_S \nabla^2\phi da = \int_\beta \frac{\partial\phi}{\partial n} ds - \int_\alpha \frac{\partial\phi}{\partial n} ds = \Phi_\beta - \Phi_\alpha,$$

where the second equality is due to Green's formula. Thus $\Phi_\beta = \Phi_\alpha$. This is still true if α and β cross each other, as can be seen by applying the same argument twice with a third loop, enclosing both α and β . Therefore the flux through a loop enclosing p is independent of the loop itself, and can be regarded as a property of the singularity p . The flux Φ from a given singularity will be called the *charge* of a singularity. Condition (1A) requires that the charge of a singularity be quantized, i.e. only have values of $k\pi/2$.

We now turn to examine the boundaries of D . Let $A, B \in \Gamma_j \setminus (J \cup P_B)$, such that the segment β of Γ_j between A and B does not contain points in $J \cup P_B$, see Fig 10. We think of A, B as being close to each other. Let α be some curve from A to B , such that no charge is enclosed in $[\alpha, \beta^-]$, where β^- is the inverse curve, defined by traversing β in the opposite direction. From

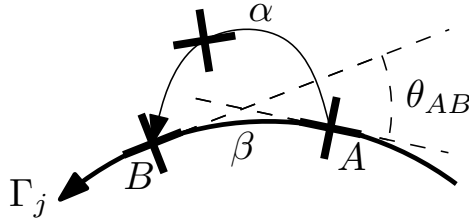


Figure 10: Condition 2.

the definition of the cross-field V it follows that the parallel-transport of $V(A)$ along α is $V(B)$, thus the parallel translate of $\mathbf{t}_A(\Gamma_j)$ along α is at angle $k\frac{\pi}{2}$ to $\mathbf{t}_B(\Gamma_j)$. Denote by θ_{AB} the angle between $\mathbf{t}_A(\Gamma_j)$ and $\mathbf{t}_B(\Gamma_j)$. Let S be the region enclosed by $[\alpha, \beta^-]$. By Green's theorem

$$\begin{aligned} 0 &= \int_S \nabla^2 \phi da = \oint_{[\alpha, \beta^-]} \frac{\partial \phi}{\partial n} ds = \int_\alpha \frac{\partial \phi}{\partial n} ds + \int_{\beta^-} \frac{\partial \phi}{\partial n} ds \\ &= \delta \theta_{\mathbf{t}_A}(\alpha) + \int_{\beta^-} \frac{\partial \phi}{\partial n} ds = k\frac{\pi}{2} + \theta_{AB} - \int_\beta \frac{\partial \phi}{\partial n} ds, \end{aligned} \quad (14)$$

with $k \in \mathbb{Z}$. By ϕ -manifold definition, (iii), $\frac{\partial \phi}{\partial n}$ is continuous and thus bounded along β , and if $B \rightarrow A$, then $\oint_\beta \frac{\partial \phi}{\partial n} ds \rightarrow 0$, thus $k = 0$. If $B \rightarrow A$, $\theta_{AB} = \oint_\beta \frac{\partial \phi}{\partial n} ds$ gives the condition:

Condition 2. For a point $A \in \Gamma_j$, $A \notin (J \cup P_B)$ the curvature $\kappa(A)$ of Γ_j at A is

$$\kappa(A) = \left. \frac{\partial \theta}{\partial s} \right|_A = \left. \frac{\partial \phi}{\partial n} \right|_A. \quad (15)$$

Condition (2) links the geometrical structure of the boundary with boundary conditions on ϕ . Its similarity to Eq. (6) is not incidental: roughly speaking, Eq. (15) ensures that geodesics close to the boundary and parallel to it follow the shape of the boundary.

The next condition will restrict the behavior of ϕ near a junction point, or a point of P_B . Let $C \in \Gamma_j$, $C \in J \cup P_B$ with inner angle θ_{in} , see Fig. 11. For $C \in P_B$, $\theta_{in} = \pi$ radians. Let α_r be a curve along the arc of the circle of radius r around C , on the inner side of Γ_j , between points A, B , see fig 11. As $r \rightarrow 0$, the angle between $V(A)$, and $V(B)$ approaches θ_{in} . Therefore, by Eq. (12), the following condition is obtained:

Condition 3. *For a curve α_r as defined above:*

$$\Phi_{\alpha_r} = \int_{\alpha_r} \frac{\partial \phi}{\partial n} ds = \delta \theta_{V(A)}(\alpha_r) \xrightarrow{r \rightarrow 0} k \frac{\pi}{2} - \theta_{in}. \quad (16)$$

Since the (Euclidian) length of α is $\theta_{in}r$, this requires a radial singularity in $\nabla \phi$ at C : $\frac{\partial \phi}{\partial r} \sim 1/r$.

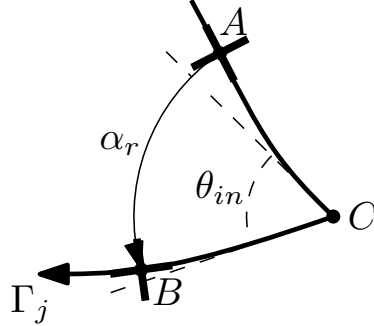


Figure 11: Condition 3.

The last requirement for a cross-field to exist is a relation between different boundary connectivity elements. Denote by Γ_1, Γ_2 two boundary curves, and by A_1, A_2 points on Γ_1, Γ_2 respectively. Let α be some curve from A_1 to A_2 , see Fig. 12. For $i = 1, 2$, $\mathbf{t}_{A_i}(\Gamma_i) \in V(A_i)$. Let θ_i be the angle between \mathbf{t}_{A_i} and the x-axis. By the cross-field definition, (ii) $V(A_1)$ is parallel translated to $V(A_2)$, so by Eq.(12) we get:

Condition 4. *The flux of $\nabla \phi$ along a curve α from $A_1 \in \Gamma_1$ to $A_2 \in \Gamma_2$ is equal to*

$$k \frac{\pi}{2} + \theta_2 - \theta_1 = \int_{\alpha} \frac{\partial \phi}{\partial n} ds = \Phi_{\alpha} \quad (17)$$

for some $k \in \mathbb{Z}$.

This is true for any curve from A_1 to A_2 , though k may vary for different curves.

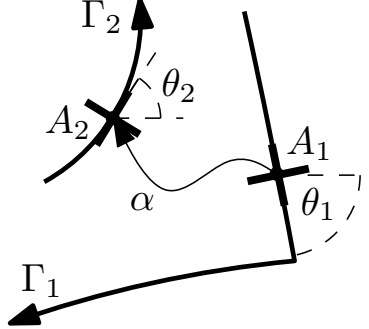


Figure 12: Condition 4.

5.1 The conditions are sufficient

In the previous section the Conditions (1A),(2),(3),(4) on the ϕ -manifold have been shown to be necessary for the existence of a cross-field. The following theorem shows that together they are sufficient. The theorem also shows how to construct the cross-field given the ϕ -manifold.

Theorem 9 *Let $A_0 \in \Gamma_{j_0}$ be some boundary point such that $A_0 \notin J \cup P_B$. Assume ϕ satisfies Conditions (1A),(2),(3), and Condition (4) with curves ε_i between A_0 and points E_i on every boundary Γ_i , $i \neq j_0$. Let $V(A_0)$ be the (unique) cross such that $\mathbf{t}_{A_0}(\Gamma_{j_0}) \in V(A_0)$. For every $B \in D \setminus P$, let α be some curve from A_0 to B , and define $V(B)$ to be the translate of $V(A_0)$ along α . Then $V(B)$ is independent of α , and V is a cross-field.*

The proof is given in Appendix C.

6 Cell Size

In the previous section a structure giving the “local direction” of edges in a mesh was developed. The directions of edges are closely related to the changes in cell-size throughout the mesh. This relation, and the notion of “local cell size”, are the subject of this section. Recall that the differential of the distance on a manifold is given by (see Notation 2.1)

$$dl^2 = dx^i g_{ij} dx^j.$$

For a ϕ -manifold, where $g_{ij} = e^{2\phi} \delta_{ij}$ this becomes

$$dl = e^\phi \sqrt{(dx^1)^2 + (dx^2)^2} = e^\phi ds. \quad (18)$$

The length of a curve in a manifold is given by

$$L(\alpha) = \int_{\alpha} dl = \int_{\alpha} e^\phi ds. \quad (19)$$

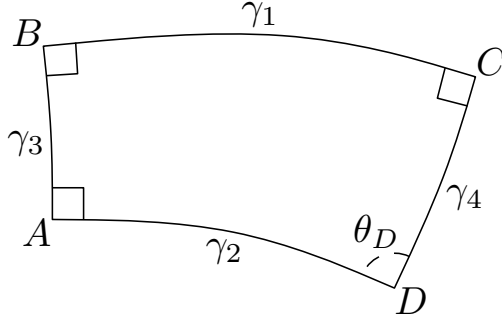


Figure 13: A geodesic “rectangle”.

The area of a region R in a manifold M is

$$A_M(R) \equiv \int_R \sqrt{g} dx^1 dx^2 = \int_R e^{2\phi} dx^1 dx^2 \quad (20)$$

where $g = \det(g_{ij})$, and the second equality holds specifically in the case of a ϕ -manifold.

The following is true for any manifold that is flat (i.e. curvature tensor zero) in some region. It is the “manifold version” of the properties of a rectangle, and follows directly from the isometry of a flat manifold and the Euclidian plane.

Claim 10 *Let $\gamma_1, \gamma_2, \gamma_3, \gamma_4$ be 4 geodesic segments in a flat region of a manifold, organized as in Fig. 13, and suppose the inner angles at the vertices A, B, C are right angles. Then the inner angle at D , θ_D , is a right angle, and $L(\gamma_1) = L(\gamma_2), L(\gamma_3) = L(\gamma_4)$, where $L(\gamma_i)$ is the manifold-length of the i -th side of the “rectangle”. The area of the “rectangle” is $L(\gamma_1) \cdot L(\gamma_3)$.*

In an Euclidian plane, the properties of a rectangle allow one to lay a grid on a region of the plane. A grid can be thought of as two families of mutually perpendicular straight lines, with equal spacing between the lines. The same can be done for a ϕ -manifold using the “rectangle” properties stated in claim 6.1, see Fig. 14. The grid divides the space into square-like regions, each bounded by 4 geodesic segments of manifold length ΔL , that will be called *manifold-edges*. The regions enclosed by the manifold-edges will be called *manifold-cells*.

According to Eq. (18), The Euclidian distance along a manifold-edge γ_e is given by

$$\Delta s(\gamma_e) = \int_{\gamma_e} e^{-\phi} dL. \quad (21)$$

The Euclidian size of the manifold-cells can thus be controlled by adding a constant to ϕ , without violating the Conditions of section 5 (i.e., without changing the C-frame). Therefore, overall cell-size can be controlled by adding a constant to ϕ while keeping ΔL fixed, and we will henceforth assume that $\Delta L = 1$. For

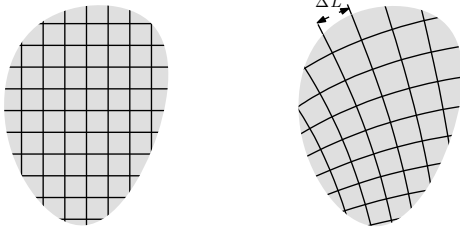


Figure 14: A grid on an Euclidian plane (left), and on a flat manifold (right).

small enough manifold cells (large enough ϕ), $\Delta s(\gamma_e) \simeq e^{-\phi}$. This leads to the interpretation of $e^{-\phi}$ as the *local edge length*, or *local cell size*.

If a mesh is to be composed of cells corresponding to the manifold-cells, e.g. by using the vertices of the manifold-cells as the vertices of the triangles or quadrilaterals, it is required that the number of manifold cells be finite. This will further restrict the type of ϕ -singularity allowed at a point p , as we will now see.

Let B be a neighborhood of a singularity, which for convenience we assume is at $r = 0$, i.e. $\nabla^2\phi(r) = 0$ for $r \in B \setminus \{0\}$. The general form of solution of the Laplace equation can be written in polar coordinates (r, ψ) as⁶:

$$\phi(r, \psi) = \phi_L + \frac{Q}{2\pi} \ln r + \sum_{n=1}^{\infty} b_n r^{-n} \sin(n\psi + c_n), \quad (22)$$

where ϕ_L is a solution to the Laplace equation $\nabla^2\phi_L = 0$ in B (including $r = 0$), and $\{b_n\}_{n=1}^{\infty}, \{c_n\}_{n=1}^{\infty}$ are sets of real numbers.

For ϕ given by Eq. (22), the flux of $\nabla\phi$ through a loop around $r = 0$ is

$$\Phi = \oint \frac{\partial \phi}{\partial n} ds = Q,$$

and using Condition (1A) we find

$$Q = k\pi/2$$

for some $k \in \mathbb{Z}$.

We now demand that the number of manifold-cells near p be finite. Since a manifold-cell has unit area, the number of manifold-cells in a region is equal to its area. The manifold area of a disc B_R of radius R around p is obtained by

⁶See Ref. 14, Eq. (2.71). The term $a_0 + \sum_{n=1}^{\infty} a_n \rho^n \sin(n\psi + \alpha_n)$ in the reference is denoted here by ϕ_L .

substituting Eq. (22) into Eq. (20)

$$\begin{aligned} A_M(B_R) &= \int_{B_R} e^{2\phi} dx^1 dx^2 = \int_0^R \exp \left(2\phi_L + \frac{k}{2} \ln r + \sum_{n=1}^{\infty} b_n r^{-n} \sin(n\psi + c_n) \right) 2\pi r dr \\ &= 2\pi \int_0^R r^{k/2+1} \exp \left(\sum_{n=1}^{\infty} b_n r^{-n} \sin(n\psi + c_n) \right) e^{2\phi_L} dr \end{aligned} \quad (23)$$

since the solution of $\nabla^2 \phi_L = 0$ is bounded in a compact region, $e^{2\phi_L}$ does not effect the convergence of the integral. To converge, it is required that $b_n = 0$ for every n , and that $k > -4$. This restricts ϕ to the form

$$\phi(r) = \phi_L + \frac{k}{4} \ln r. \quad (24)$$

with $k > -4$. This is a solution of the Poisson equation for one point-source $\nabla^2 \phi = k\pi/2\delta^{(2)}(r)$ in a neighborhood of $r = 0$. For many singularities, this gives a more restricted version of Condition (1A) (Note that the sum of solutions to the Laplace equation is also a solution):

Condition 1B. For $r \in D \setminus P$, $\phi(r)$ can be written as

$$\phi(r) = \phi_L + \frac{1}{4} \sum_{i=1..N} k_i \ln(|r - p_i|),$$

with $k_i > -4$, $P = \{p_i\}_{i=1..N}$, and $\nabla^2 \phi_L = 0$ on D . Or, what is equivalent, ϕ obeys the equation

$$\nabla^2 \phi(r) = \frac{\pi}{2} \sum_{i=1..N} k_i \delta^{(2)}(r - p_i),$$

the Poisson equation with point sources, with $k_i \in \mathbb{Z}$, $k_i > -4$.

Fig. 15 shows selected C-frame geodesics around a singularity (with $\phi_L = 0$), spaced at manifold-distances of $\Delta L = 1$ from each other, for different singularity strengths. In practice, good candidates for meshes will only have singularities of charge $k \geq -1$, due to the inner-angles of cells incident on the singularity, see also Remark 1 in section 7.2 below.

7 Discussion: Finding a ϕ -manifold

According to theorem 1 in section 5.1, if a ϕ -manifold is found, adhering to Conditions (1A),(2),(3),(4), a C-frame exists, and can be found. In section 6 Condition (1A) was further restricted, yielding Condition (1B).

In addition to conditions (1B),(2),(3),(4), a meshing problem can include other requirements, such as cell size demand on the boundaries, or inside the mesh. Clearly, finding an appropriate ϕ -manifold then depends on these conditions as well. In what follows the problem of finding a ϕ -manifold under different

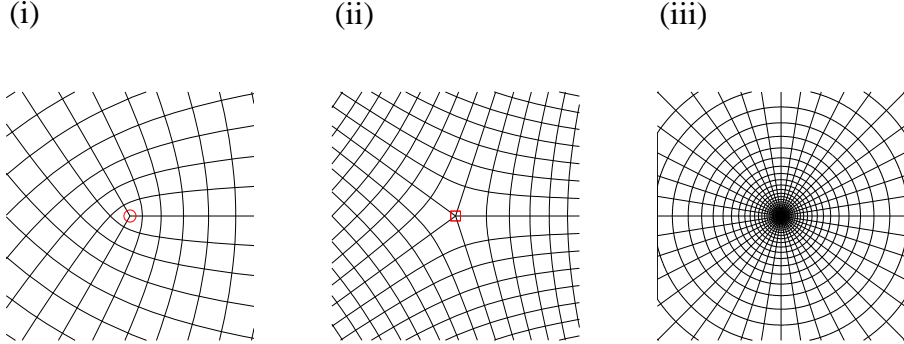


Figure 15: C-frame geodesics around a singularity. The geodesics are placed at unit manifold-distances apart. (i) A $k = -1$ singularity. (ii) A $k = 1$ singularity. (iii) A $k = -4$ singularity, with an infinite number of cells.

requirements will be discussed, starting with simpler cases, and progressing to more complex, general situations.

After finding a valid ϕ -manifold, the final stage of a mesh generation process involves finding a discrete partition into well-shaped manifold cells, see below. A comprehensive discussion will not be given here, but some comments on this process will be made as part of the case studies.

7.1 Case Study A: No singularities are needed

We start with a simple case. Suppose that the boundary has one connectivity element (loop) Γ_1 . Further, suppose that all junction angles θ_{Ji} (equal to $\pi - \theta_{in}$, the inner angle) are multiples of $\pi/2$, and that the their sum is $\sum_i \theta_{Ji} = 2\pi$. In such a case, Condition (4) is empty (since there is only one boundary loop), and Condition (3) can be satisfied with $k_i = 1$, and without any additional radial-singularities at the junction points. Condition (2) are Neumann boundary conditions on ϕ . Γ_1 is a simple loop, and the sum of junction angles is 2π , thus the total is flux of ϕ through the boundary is

$$\Phi_{\Gamma_1} = \int_{\Gamma_1} \frac{\partial \phi}{\partial n} ds = \int_{\Gamma_1} \kappa ds = 2\pi - \sum_i \theta_{Ji} = 0.$$

Therefore given the boundary conditions a solution to the Laplace equation (that is, with no singularities) exists, and is unique up to an additive constant [13].

A simple example of such a case, that can be solved analytically, is a section of a ring between two radial lines, see Fig. 16. The boundary conditions on the sides of the boundary, dictated by the shape of the boundary are given,

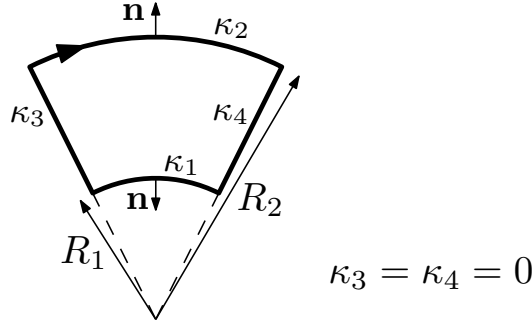


Figure 16: The boundary specified in Eq. (25).

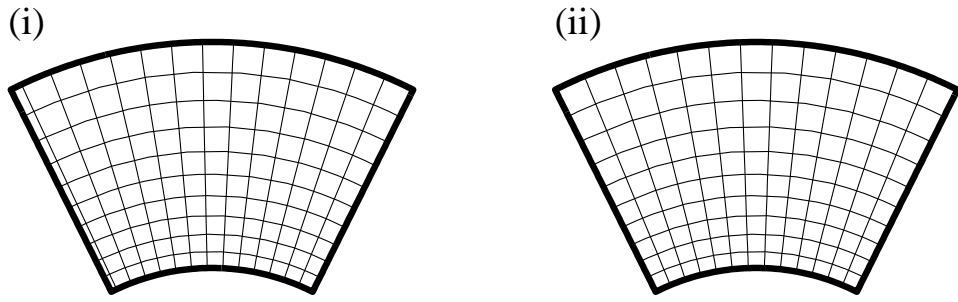


Figure 17: C-frame geodesics for the example in Fig. 16. (i) equally-spaced geodesics. (ii) geodesics forming well-shaped manifold cells.

according to Condition 2, by (note that κ can be negative, see Eq. (6)):

$$\begin{aligned} \left. \frac{\partial \phi}{\partial n} \right|_1 &= \kappa_1 = \frac{1}{R_1} \\ \left. \frac{\partial \phi}{\partial n} \right|_2 &= \kappa_2 = -\frac{1}{R_2} \\ \left. \frac{\partial \phi}{\partial n} \right|_3 &= \left. \frac{\partial \phi}{\partial n} \right|_4 = 0. \end{aligned} \tag{25}$$

The solution to the Laplace equation $\nabla^2 \phi = 0$ with boundary conditions given in Eq. (25) is

$$\phi = -\ln r + C'. \tag{26}$$

Here, r is the distance from the center of the ring, and C' is a constant. Note that no specification of the local cell size was given in the input, and, according to section 6, the resulting local cell-size function is part of the solution. It is given by $\exp(-\phi) = Cr$, with $C \equiv -\ln C'$.

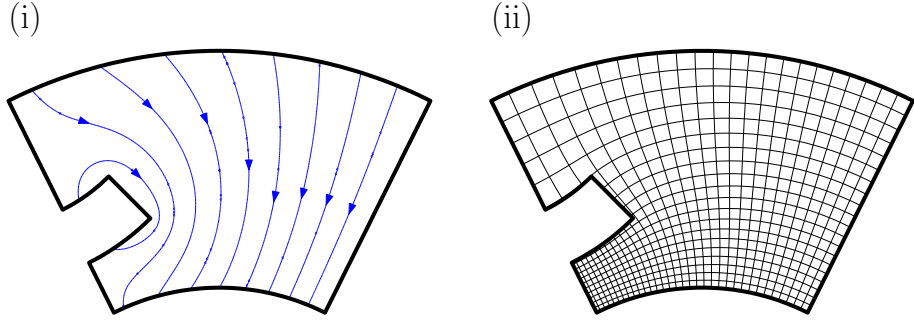


Figure 18: A more elaborate example than that of Eq. (25). (i) Flow-lines of $\nabla\phi$. (ii) Equally-spaced geodesics.

Fig. 17 shows geodesics starting from the boundaries. They were calculated by solving the geodesic equation, Eq. (5), with initial velocity perpendicular to the boundary. The integration constant C was chosen such that 10 manifold-edges will fit on the radial boundaries, i.e. that $\int_{R_1}^{R_2} e^\phi dr = 10$. This fixes the solution completely, and gives a non-integer manifold-length along the arcs. Fig. 17,(i) shows spaced at unit manifold-distances of each other. Whereas the radial direction fits exactly 10 manifold-edges of equal length, the manifold-distance from the left-most geodesic to the boundary is less than 1, resulting in manifold cells with high aspect ratio. In Fig. 17, (ii), two different spacings are used, so as to allow equal spacing in both the radial and tangential directions, with an aspect ratio as close to one as possible. Fig. 18 shows an example with a more elaborate boundary adhering to the restrictions stated in the beginning of section 7.1. Again, the equally-spaced geodesics of Fig. 18,(ii) do not form well-shaped (or even valid) cells. A valid discretization can be created, e.g. by using geodesics emanating from the junction points to decompose the domain.

We now lift the restriction that all junction angles are multiples of $\pi/2$. If the angle is not $\pi/2$, Condition (3) requires that ϕ have a radial-singularity at the junction point. Let the junction inner-angle be θ_{in} . Suppose that ϕ contains a singularity caused by placing a charge at the junction point, i.e. $\phi = \frac{Q}{2\pi} \ln r$. (If two or more boundary segments are incident on the same point, other techniques may be required.) Let α_r be the curve formed by traversing an arc of the circle as in Fig. 11. then according to Eq. (16)

$$\frac{\pi}{2}k - \theta_{in} = \int_{\alpha_r} \frac{\partial \phi}{\partial n} ds = \frac{Q}{2\pi r} \theta_{in} r = \frac{Q}{2\pi} \theta_{in},$$

thus

$$Q = 2\pi \left(k \frac{\pi/2}{\theta_{in}} - 1 \right) \quad (27)$$

for some $k \in \mathbb{Z}$. k must be positive, since otherwise $Q \geq 2\pi$, and the manifold-area diverges at the singularity, by the same argument as the one following Eq.

(20). Apart from this restriction the number k is not fixed, and affects the manifold-angle at the singularity, i.e. the number of manifold-cells incident on the junction.

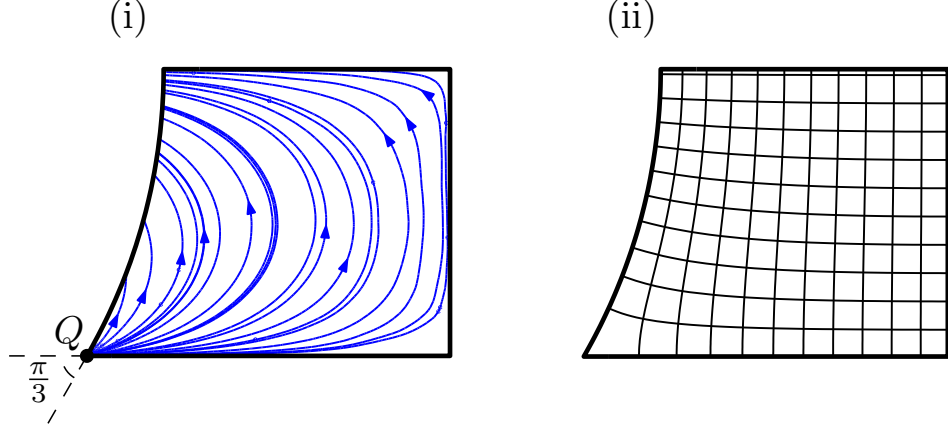


Figure 19: A domain with a singularity at a junction point.

The example in Fig. 19 shows a domain enclosed by one boundary element. In one junction, the inner angle is $\pi/3$, which, according to Eq. (27), requires a singularity of charge $Q = \pi$, for $k = 1$ placed at the junction. The solution was calculated by decomposing ϕ into 2 contributions: $\phi = \phi_c + \phi_L$. ϕ_c is the charge potential, $\phi_c = \frac{Q}{2\pi} \ln r$. ϕ_L was computed by numerically solving the Laplace equation with boundary conditions $\frac{\partial \phi_L}{\partial n} = \frac{\partial \phi}{\partial n} - \frac{\partial \phi_c}{\partial n}$.

The examples that were presented in this case study could have been obtained by a conformal mapping from a “logical” domain. This is, of course, not true when defects are present inside the domain⁷. Note, however, that unlike many mapping techniques, even when the “logical” domain can be defined, it is *not fixed in advance, and is part of the solution*. This is even more pronounced in problems involving defects, see below. Conformal mappings that are also boundary aligned are quite limited in the scope of problems they can mesh, and sometimes yield large differences in cell size (as in the example shown in Fig. 18). In mapping techniques, therefore, the conformal restriction is lifted, see e.g. Ref. 2. In the present work, the conformal condition (in its manifold formulation) is kept, and instead defects are allowed into the manifold.

⁷Even without defects inside the domain, this is not always possible, since the mapping from D to the “logical” domain is not, in general, one-to-one. In manifold-theory terminology, even if the manifold is flat and simply connected, it is not necessarily covered by a single conformal coordinate patch.

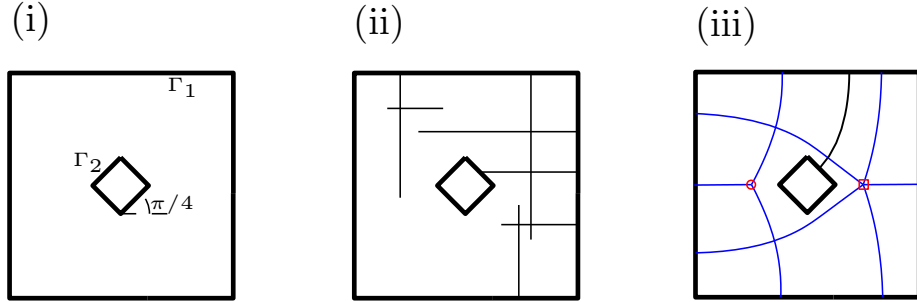


Figure 20: The significance of Condition (4). (i) The input boundary. (ii) Ignoring Condition (4), $\phi = \text{const}$ is a possible manifold. The resulting C-frame does not conform with all boundaries. (iii) A manifold with two singularities. Selected geodesics are drawn.

7.2 Case Study B: Two boundaries, no boundary cell-size demand

The purpose of the following example is to demonstrate the meaning and importance of Condition (4). Unlike the other Conditions, the formulation of Condition (4), stating the required relations between different boundary elements, is not local. We now show that the relative placement of different boundary elements can force the introduction of defects (conical singularities) in order to obtain a valid C-frame.

Fig. 20,(i) shows a domain bounded by two boundary elements, an “outer loop” Γ_1 , and an “inner loop” Γ_2 . Assume that there are no demands on cell-size. We start by ignoring Condition (4), and trying to proceed as in Case A, that is, searching for a solution without defects. The curves composing Γ_1, Γ_2 are straight lines, so the Neumann boundary conditions read $\frac{\partial \phi}{\partial n} = 0$, and the solution to the Laplace equation is trivial: $\phi = \text{const}$. Condition (3) is also fulfilled with $k = 1$ at all junctions. However, this solution does not give a valid C-frame. A C-frame geodesic running from Γ_1 to Γ_2 will not reach Γ_2 at a right angle, see fig. 20,(ii). Thus, we cannot do without Condition (4), and since the only solution without defects with boundary conditions $\frac{\partial \phi}{\partial n} = 0$ is $\phi = \text{const}$, we learn that a solution without defects does not exist. One possible solution with defects is shown in Fig. 20,(iii). This solution, obtained using symmetry arguments, contains two defects with opposite signs. Selected geodesics of the C-frame are shown in 20,(iii). Of them, one geodesic runs from one boundary to the other. The rest are geodesics that are incident on the defects.

Remark 11 *In Fig. 20,(iii), C-frame geodesics reaching the defects are shown. Three C-frame geodesics reach the left defect, which has a charge of $k = -1$, and five reach the right defect, which has a charge of $k = 1$. Moreover, it seems they reach the defects at equally distributed angles. These observations are true*

in general. It can be proved that there are always exactly $k+4$ angles from which C-frame geodesics are incident upon a singularity, and these angles are equally distributed around the singularity. Such geodesics will be called star-geodesics. Note that this affects the angles of the mesh-cells created: for small cells with a defect on one vertex, that vertex's inner angle will be approximately $\frac{2\pi}{k+4}$.

7.3 Case Study C: boundary cell-size demand; finding defects locations

In Case Studies A,B above no constraint on the size of boundary edges was given. Yet the boundary edge-length is often specified in meshing problems. Suppose we are given a function F stating the required cell size (that is, cell edge length) at each point on the boundary. The local cell size is $e^{-\phi}$, thus $F = e^{-\phi}$, giving a Dirichlet boundary condition on ϕ :

$$\phi|_{\Gamma} = -\ln F. \quad (28)$$

Condition (1B) states that ϕ obeys a Poisson equation with point charges playing the role of defects. The problem of finding a suitable ϕ is reduced to finding a charge distribution (number of charges, their locations and charge-strengths), such that ϕ will fulfill Conditions (2),(3),(4), together with Eq. (28). This is an *Inverse Poisson (IP)* problem. As opposed to a Direct Poisson problem, where the charge-distribution ρ in $\nabla^2\phi = \rho$ is known, and one is asked to find ϕ , in an IP problem, *certain information on ϕ is given, and the charge distribution ρ is to be found*.

IP problems have important applications in various areas of science and engineering [16]-[20]. By its nature, the IP problem is ill-posed, and the solution may not be unique, and may be sensitive to small changes of the input, such as small changes in boundary conditions. In problems of this type any a-priory information on the charge distribution can play an important role in the solution of the problem.

The problem of finding ϕ can be broken into the following steps:

- (i) Given the boundaries Γ_i of the domain, and the cell-size requirement F on the boundary, calculate the Neumann boundary conditions $\frac{\partial\phi}{\partial n}\Big|_{\partial D} = \kappa$ (Condition (2)), and Dirichlet boundary condition $\phi|_{\partial D} = -\ln(F)$ (Eq. (28)).
- (ii) Impose boundary condition (3), e.g. by placing charges at the junction points (see Eq. (27)).
- (iii) Solve the IP problem: Find the (finite) number, location and strength of charges such that Neumann and Dirichlet boundary conditions calculated in (i), and Condition (4) hold approximately (See Remark 2,(i) below). According to Condition (1B), the charges should be of strength $k_i\pi/2$, with $k_i > -4$, (see Remark 2,(ii)). The charges can be placed:

1. (a) Inside D (the set P).
- (b) In junction points (which amounts to changing k in Eq. (27)).
- (c) On the rest of the boundary (the set P_B), where according to Eq. (27) with $\theta_{in} = \pi$, charges of strength $k_i\pi$ can be placed.
- (iv) Once the charges are placed, ϕ is found by solving the standard (Direct) Poisson problem.

Remark 12 (i) Note that since this is an inverse problem, i.e. the charge distribution is not fixed, both Neumann and Dirichlet boundary conditions can be imposed.

(ii) Though the limit on k_i due to Condition (1B) is $k_i > -4$, charges should be of charge $k_i \geq -1$ in order to have convex cells, and preferably with $k_i \leq 2$. This is due to inner angles of cells incident on the singularity, see Remark 1 in section 7.2.

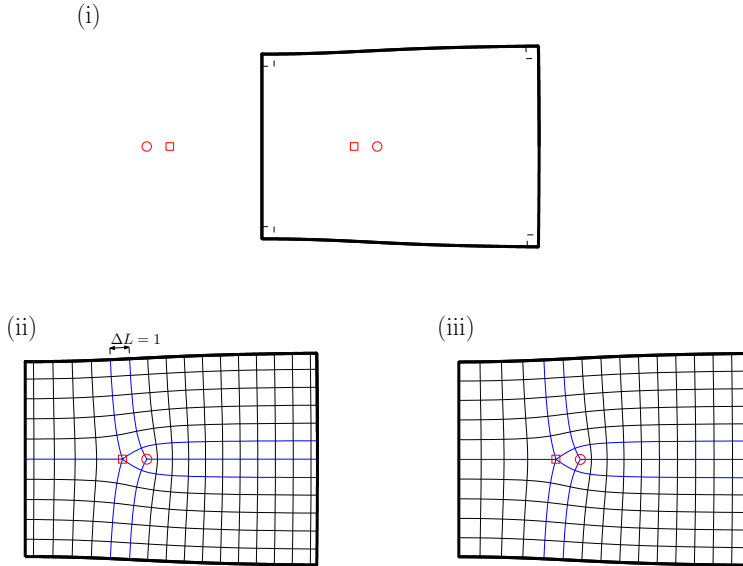


Figure 21: The steps of a possible mesh-generation process. (i) The input boundary (Thick line). Locations of singularities of ϕ_0 that was used to create the boundary are marked. (Square: $k = 1$, Circle: $k = -1$). (ii) A solution recovered using an IP algorithm (see text). Reconstructed singularities marked as in (i). Equally-spaced geodesics are shown (thin lines). (iii) Geodesics of the reconstructed solution, at approximately equal spacings.

The steps outlined above are illustrated in Fig. 21. For the purpose of this example, a boundary was created artificially by joining four geodesics of a ϕ field, at right angles to each other. The ϕ -field chosen for creating the boundary

is a sum of fields from four charges: $\phi_0(r) = \sum_{i=1}^4 k_i \frac{\pi}{2} \ln |r - r_i|$, with k_i, r_i the charges' strengths and locations. Two charges are located inside the boundary, and two outside, see Fig. 21,(i). This defines the shape of the boundary. The cell size demand imposed on the boundary was $F = e^{-\phi_0}$, plotted in Fig. 22. The boundary shape and the cell size demand complete the problem's input.

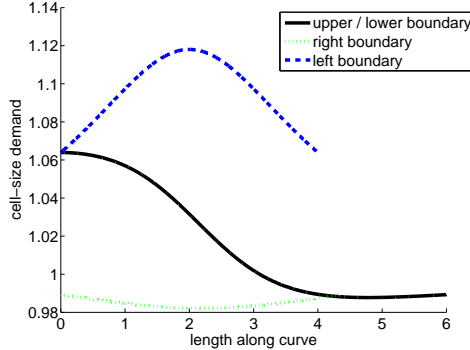


Figure 22: The cell-size input demand along the four sides of the boundary shown in Fig. 21,(i). The upper / lower boundary curves are traced from left to right.

Using this input, the steps of the algorithm outlined above were followed. First (step (i)), Neumann and Dirichlet boundary conditions were calculated from the input. Step (ii) was fulfilled automatically without adding additional charges, because all junction have right inner angles. In step (iii) an algorithm solving the IP problem [21] was invoked. The algorithm exactly reconstructed the location and charge of the two charges inside the domain. (It is important to note that the IP algorithm of [21] could be used directly due to the artificial nature of the problem: the input was constructed such that these two charges will reconstruct the input conditions exactly. This may not be the case in other cases, and may require other IP solution methods.) The ϕ -field was then constructed by solving the *direct*, standard Poisson problem, with *given* charges. In this example, since the location and structure of the charges inside the domain were recovered exactly, the ϕ recovered was exactly ϕ_0 .

Fig. 21,(ii) shows C-frame geodesics at equal manifold-distances $\Delta L = 1$. As was discussed in section 6, the function ϕ is defined up to an additive constant, that controls the overall cell-size. This constant was chosen such that the manifold-distance ΔL between two geodesics incident on the two charges be equal to one, see Fig. 21,(ii). In Fig. 21,(iii) C-frame geodesics spaced at approximately equal manifold-distances are shown, such that no high aspect-ratio manifold cells, as those in Fig. 21,(ii), exist. Note that the star-geodesics divide the domain into sub-domains without charges, that can be meshed more easily. This hints at possible ways of using the ϕ -manifold for creating meshes.

7.4 Other cases

Other mesh-demands can be formulated. Examples include cell-size within the domain (as in adaptive meshing), and cell direction. We comment shortly on these subjects. In the case of adaptive meshing, a demand for cell size F as a function of location inside the domain is given. This is translated to a demand on ϕ by $\phi = -\ln(F)$. This fixes ϕ completely, and therefore may not be fulfilled exactly along with other conditions, such as having $\nabla^2\phi = 0$ almost everywhere. However, weaker constraints may be given, such as specifying F along curves within the domain. In the case of cell direction, a demand on the direction of geodesics, that is, the direction of the cross-field, is given. This translated to a constraint similar to Condition (4), on the flux Φ through some arbitrary curve. As is the case with adaptive meshing, a requirement for cell direction everywhere inside the domain is too restrictive, but more limited demands, such as a demand on selected points inside the domain may be made.

8 Conclusions

In this work a continuum description of unstructured meshes was proposed. The two components of this structure are a Riemannian manifold, completely defined by a real function ϕ , and a family of geodesic-curves on that manifold, called the C-frame. The edges of the mesh are to be laid along the C-frame curves, spaced at distances fixed by the function ϕ , thus creating the mesh cells. The structure aims at describing meshes that, away from irregular vertices, have well-shaped cells. In the limit of an increasingly finer mesh, the cell's shape approaches the shape of a square (in the case of a quadrilateral mesh) or equilateral triangle (for triangle meshes). After fixing the behavior of the mesh away from irregular vertices, the focus turns to the irregular vertices, represented in the continuum structure by defects, i.e. conical singularities.

The demand that the mesh conform to the boundary yields conditions on the function ϕ . The resulting reduced problem is an Inverse Poisson problem, of finding a distribution of localized charges adhering to these conditions. The charges correspond to defects.

The main component needed to utilize the theory to mesh generation is a suitable Inverse Poisson algorithm. An algorithm for creating the final discrete mesh is also required.

9 Acknowledgements

I am indebted to Dov Levine for introducing me to the theory of defects, and for his continuing support. Helpful discussions with Shlomi Hillel and Craig Gotsman are much appreciated.

A The Curvature Tensor

In Riemannian geometry, the Christoffel symbols are related to the metric tensor by

$$\Gamma_{ij}^l = g^{kl} \left(\frac{\partial g_{ik}}{\partial x^j} - \frac{\partial g_{ij}}{\partial x^k} + \frac{\partial g_{kj}}{\partial x^i} \right).$$

where g_{ij} is the metric, and g^{kl} is defined as the (k, l) entry in the matrix inverse of g_{ij} . The curvature tensor is given as a function of the Christoffel symbols by

$$R_{i\ jk}^l = (\Gamma_{ik}^l)_{,j} - (\Gamma_{ij}^l)_{,k} + \Gamma_{ik}^p \Gamma_{pj}^l - \Gamma_{ij}^p \Gamma_{pk}^l.$$

where the comma denotes differentiation: $(\)_{,j} \equiv \partial/\partial x^j$. In a flat manifold $R_{i\ jk}^l = 0$. In two-dimensions $R_{i\ jk}^l$ has just one independent component, $R_1^2{}_{12}$. Eq. (1) in section 2 is derived by substituting $g_{ij} = e^{2\phi} \delta_{ij}$, $g^{ij} = e^{-2\phi} \delta^{ij}$ into $R_1^2{}_{12} = 0$, and after tedious but straight-forward algebraic manipulation arriving at

$$0 = \phi_{,11} + \phi_{,22}.$$

This is the Laplace equation for ϕ .

Eq. (1) can also be derived using the results of section 3 (which do not rely on Eq. (1)), and the Gauss-Bonnet theorem, which relates the parallel transport of a vector along a closed curve to the curvature inside the enclosed region [10]. According to the Gauss-Bonnet formula, on a flat manifold (i.e. $R_{i\ jk}^l = 0$ everywhere) the angular variation of a vector along a closed loop α is zero: $\delta\theta_y = 0$. Using Eq. (12) this is equal to

$$\delta\theta_y = \oint_{\alpha} \frac{\partial\phi}{\partial n} ds.$$

This can be turned into a surface integral using Green's theorem,

$$\oint_{\alpha} \frac{\partial\phi}{\partial n} ds = \int_S \nabla^2 \phi da,$$

where S is the region enclosed by α . We thus have $\int_S \nabla^2 \phi da = 0$. Since is true for *any* region S , it follows that $\nabla^2 \phi = 0$ everywhere on the manifold.

B Triangular Meshes

In this appendix the changes in the definitions and results in sections 4,5, for the case of triangular meshes are outlined.

Definition 13 (Triangle C-frame) *A family F of geodesics is a **triangle continuous-frame (Triangle C-frame)** if:*

- (i) Through every point $A \in D \setminus P$ passes at least one geodesic $\gamma_1 \in F$, and if γ_2 is a geodesic passing through A , then $\gamma_2 \in F$ if and only if the tangents of γ_1, γ_2 at A form an angle of $k\pi/3$, $k \in \mathbb{Z}$.
- (ii) If A is a point on a boundary curve Γ_j , $A \notin J \cup P_B$, and $\gamma_1 \in F$ such that $\lim_{t \rightarrow t_0} (\gamma_1(t)) = A$, then the tangents of γ_1, Γ_j at A form an angle of $k\pi/3$, $k \in \mathbb{Z}$.

The cross for a triangular mesh is has six instead of four equivalent directions. For vectors $v_1, v_2 \in \mathbb{R}^2$, $v_1 \sim v_2$ iff v_1, v_2 form an angle of $k\pi/3$, $k \in \mathbb{Z}$. As in the quadrilateral case, a **cross** is an element of \mathbb{R}^2 / \sim . The definition of a cross-field is the same as for the quadrilateral case.

The conditions for the existence of a Triangle C-frame read:

Condition 1A. Eq. (13) for the triangular case is

$$k\pi/3 = \delta\theta_y = \Phi.$$

Condition 2. Is the same as in the quadrilateral case.

Condition 3. for the triangular case reads

$$\int_{\alpha_r} \frac{\partial \phi}{\partial n} ds = \delta\theta_{V(A)}(\alpha_r) \xrightarrow{r \rightarrow 0} k\frac{\pi}{3} - \theta_{in}.$$

Condition 4. Eq. (17) of becomes

$$k\frac{\pi}{3} + \theta_1 - \theta_2 = \int_{\alpha} \frac{\partial \phi}{\partial n} ds = \Phi_{\alpha}.$$

Finally, Condition (1B) for triangular meshes reads:

Condition 1B. For $r \in D \setminus P$, ϕ can be written as

$$\phi(r) = \phi_L + \frac{1}{6} \sum_{i=1..N} k_i \ln(|r - p_i|),$$

with $k_i > -6$, and $P = \{p_i\}_{i=1..N}$. Or, what is equivalent, ϕ obeys the equation

$$\nabla^2 \phi(r) = \frac{\pi}{3} \sum_{i=1..N} k_i \delta^{(2)}(r - p_i),$$

the Poisson equation with point sources, with $k_i \in \mathbb{Z}$, $k_i > -6$.

Fig. 23 shows selected Triangle C-frame geodesics around a singularity (with $\phi_L = 0$), spaced at manifold-distances of $\Delta L = 1$ from each other, for different singularity strengths.

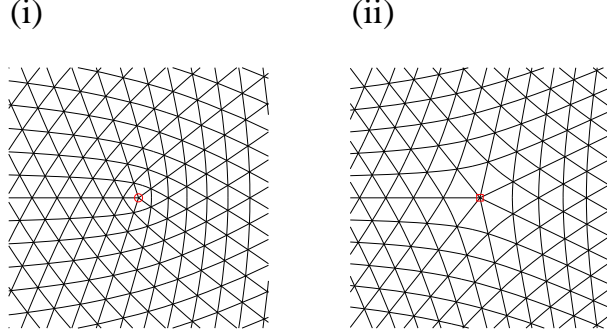


Figure 23: Triangle C-frame geodesics around a singularity. The geodesics are spaced at unit manifold-distances. (i) A $k = -1$ singularity. (ii) A $k = 1$ singularity.

C Proof of Theorem 9

Proof. We first prove that $V(B)$ for some $B \in D \setminus P$ is independent of α . Let α_1, α_2 be two curves from A_0 to B . Denote $\mathbf{t}_{A_0} \equiv \mathbf{t}_{A_0}(\Gamma_{j_0})$. We need to show that the parallel transport of \mathbf{t}_{A_0} to B gives vectors that belong to the same cross, i.e.

$$\delta\theta_{\mathbf{t}_{A_0}}(\alpha_1) = \delta\theta_{\mathbf{t}_{A_0}}(\alpha_2) + \frac{\pi}{2}k \quad (29)$$

for some $k \in \mathbb{Z}$. Using Eq. (12), Eq. (29) becomes

$$\frac{\pi}{2}k = \int_{\alpha_1} \frac{\partial\phi}{\partial n} ds - \int_{\alpha_2} \frac{\partial\phi}{\partial n} ds = \oint_{\alpha} \frac{\partial\phi}{\partial n} ds \quad (30)$$

where $\alpha \equiv [\alpha_1, \alpha_2^-]$. We now prove Eq. (30). The region enclosed by α can contain singularities and inner-boundary curves. Surround them by additional curves, as shown in Fig. 24. Denote the region between the α curve and the ω and ψ curves as S . Since $\nabla^2\phi = 0$ everywhere in S , and $\frac{\partial\phi}{\partial n}, \phi$ are finite on the boundary of S , (due to ϕ -definition, (iii)) Green's theorem can be applied to this case, giving

$$0 = \int_S \nabla^2\phi da = \oint_{\alpha} \frac{\partial\phi}{\partial n} ds + \sum_{i=1..N_{\omega}} \oint_{\omega_i} \frac{\partial\phi}{\partial n} ds + \sum_{j=1..N_{\psi}} \oint_{\psi_j} \frac{\partial\phi}{\partial n} ds \quad (31)$$

where N_{ω}, N_{ψ} are the number of points in P and inner-curves enclosed by α , respectively. We now focus on a single loop ψ_r around an inner curve Γ_r , $1 \leq r \leq N_{\psi}$. ψ_r is composed of curves η_i around points of $J \cup P_B$, and curves ζ_i between junctions, i.e. $\psi_r = [\eta_1, \zeta_1, \eta_2, \zeta_2, \dots]$, see Fig. 24. The total flux

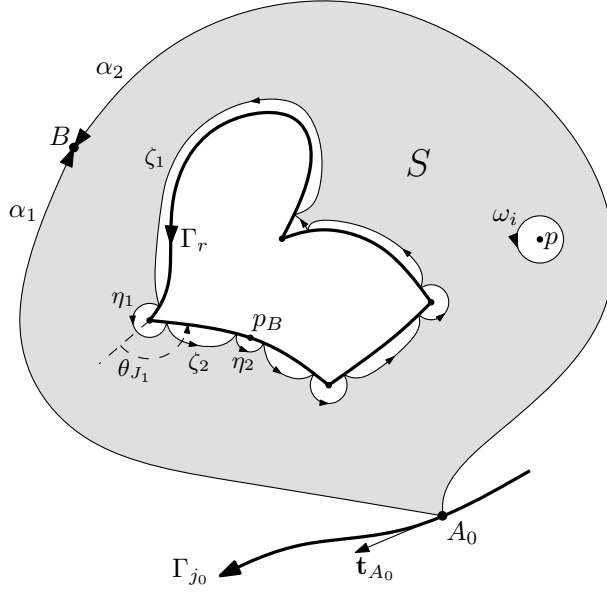


Figure 24: The cross-field is well defined.

through ψ_r is given by

$$\begin{aligned} \oint_{\psi_r} \frac{\partial \phi}{\partial n} ds &= \sum_i \oint_{\eta_i} \frac{\partial \phi}{\partial n} ds + \oint_{\zeta_i} \frac{\partial \phi}{\partial n} ds = \sum_i \theta_{in_i} + k_{J_i} \frac{\pi}{2} + \oint_{\zeta_i} \kappa ds = \quad (32) \\ &= \sum_i \theta_{J_i} - \pi + k_{J_i} \frac{\pi}{2} + \oint_{\zeta_i} \kappa ds = 2\pi + \sum_i -\pi + k_{J_i} \frac{\pi}{2} = k_{\psi_r} \frac{\pi}{2} \end{aligned}$$

with $k_{J_i}, k_{\psi_r} \in \mathbb{Z}$. The second equality uses Conditions (2),(3). The second to last equality holds because Γ_r is a simple curve with rotation index 1, so $\sum_i \theta_{J_i} + \oint_{\zeta_i} \kappa ds = 2\pi$. The flux through ω_i is given by Condition (1) to be

$$\oint_{\omega_i} \frac{\partial \phi}{\partial n} ds = k_{\omega_i} \pi / 2. \quad (33)$$

Substituting Eq. (32),(33) into Eq. (31), Eq. (31) becomes

$$0 = \oint_{\alpha} \frac{\partial \phi}{\partial n} ds + \sum_{i=1..N_{\omega}} k_{\omega_i} \pi / 2 + \sum_{i=1..N_{\psi}} k \pi / 2$$

thus

$$\oint_{\alpha} \frac{\partial \phi}{\partial n} ds = k \pi / 2$$

for some $k \in \mathbb{Z}$. This proves Eq. (30).

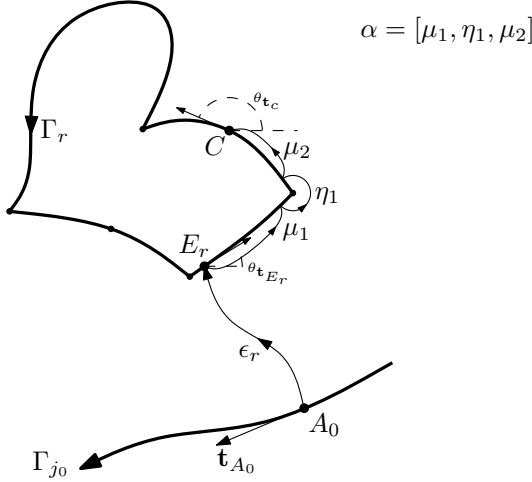


Figure 25: Boundary alignment of the cross-field.

We now turn to prove the property (ii) of a cross-field. Let C be a boundary point, $C \in \Gamma_r \setminus (J \cup P_B)$, $1 \leq r \leq N_\psi$. Since $\nabla\phi$ is continuous in the neighborhood of C , the limit $\lim_{B \rightarrow C} V(B)$ exists (we already proved $V(B)$ is well-defined). Denote $V(C) \equiv \lim_{B \rightarrow C} V(B)$. It is left to show that $\mathbf{t}_C(\Gamma_i) \in V(C)$. The assumptions of the theorem, together with Condition (4) guaranty that $\mathbf{t}_{E_r}(\Gamma_r) \in V(E_r)$. Let β be a section of Γ_r going from E_r to A . Define a curve α from E_r to A composed of curves η_n around the points of $J \cup P_B$ in the image of β , and μ_m curves between junctions, see Fig. 25.

The variation of $\mathbf{t}_{E_r}(\Gamma_r)$ along α is

$$\begin{aligned} \delta\theta_{\mathbf{t}_{E_r}}(\alpha) &= \int_{\alpha} \frac{\partial\phi}{\partial n} ds = \sum_n \int_{\eta_n} \frac{\partial\phi}{\partial n} ds + \sum_m \int_{\mu_m} \frac{\partial\phi}{\partial n} ds = \\ &= \sum_n (\theta_{J_n} - \pi) + \sum_m \int_{\mu_m} \kappa ds = \theta_{\mathbf{t}_C}(\Gamma_r) - \theta_{\mathbf{t}_{E_r}}(\Gamma_r) + k\pi/2 \end{aligned}$$

here κ is the curvature of β , and $k \in \mathbb{Z}$. The last equality expresses the fact that the change in the angle of the tangent to the boundary is the sum of the junction angles and change of angle along the curves, which is given by the integral of the curvature. Thus $\mathbf{t}_C \in V(C)$, which completes the proof of the boundary properties of V . ■

References

[1] S. J. Owen, A survey of unstructured mesh generation technology, in *Proceedings of the 7th International Meshing Roundtable*, (1998).

- [2] J. F. Thompson, B. Soni and N. P. Weatherill, *Handbook of Grid Generation* (CRC Press, 1999).
- [3] V. D. Liseikin, *A Computational Differential Geometry Approach to Grid Generation* (Springer, 2004).
- [4] V. Volterra, Sur l'équilibre des corps élastiques multiplement connexes, *Ann. Ec. Norm. Sup.* 24 (1907) 401-517.
- [5] F. R. N. Nabarro, *Theory of Crystal Dislocations* (Dover Publications, New York, 1967).
- [6] X. Gu and S. Yau, Global Conformal Surface Parameterization, *Eurographics Symposium on Geometry Processing* (2003).
- [7] L. Kharevych, B. Springborn and P. Schröder, Discrete conformal mappings via circle patterns, *ACM Transactions on Graphics* 25(2) (2006).
- [8] N. Ray, W. C. Li, B. Levy, A. Sheffer and P. Alliez, Periodic Global Parameterization, *ACM TOG*, to appear.
- [9] Y. Tong, P. Alliez, D. Cohen-Steiner and M. Desbrun, Designing quadrangulations with discrete harmonic forms, *Eurographics Symposium on Geometry Processing* (2006).
- [10] R. S. Millman and G. D. Parker, *Elements of Differential Geometry* (Prentice Hall, 1977).
- [11] M. O. Katanaev, Geometric theory of defects, *USP. FIZ. NAUK* **175** (2005) 705.
- [12] A. M. Winslow, Equipotential zoning of two-dimensional meshes, *J. Comput. Phys.* **1** (1967) 149-172.
- [13] P. R. Garabedian, *Partial Differential Equations* (John Wiley & Sons, 1964).
- [14] J. D. Jackson, *Classical Electrodynamics*, 3rd ed. (John Wiley & Sons, 1998).
- [15] J. B. Conway, *Functions of One Complex Variable I* (Springer, 1997).
- [16] M. Yamaguti et al., eds. *Inverse Problems in Engineering Sciences* (Springer-Verlag, Tokyo, 1991).
- [17] M. Hämäläinen, R. Hari, R. J. Ilmoniemi, J. Knuutila and O. V. Lounasmaa, Magnetoencephalography - theory, instrumentation, and applications to noninvasive studies of the working human brain, *Reviews of Modern Physics* **65** Issue 2 (1993) 413-497.
- [18] A. A. Ioannides et. al, Continuous probabilistic solutions to the biomagnetic inverse problem, *Inverse Problems* **6** (1990) 523-542.

- [19] P. Johnston, ed., *Computational Inverse Problems in Electrocardiography* (Southampton: WIT Press, 2001).
- [20] D. Zidarov, *Inverse Gravimetric Problem in Geoprospecting and Geodesy* (Amsterdam: Elsevier, 1990).
- [21] A. El-Badia and T. Ha-Duong, An inverse source problem in potential analysis, *Inverse Problems* **16** (2000) 651–63.